Finite element modelling of moisture related and visco-elastic deformations in inhomogeneous timber beams

Ormarsson, Sigurdur; Dahlblom, Ola

Published in:
Engineering Structures

Link to article, DOI:
10.1016/j.engstruct.2012.10.019

Publication date:
2013

Finite element modelling of moisture related and visco-elastic deformations in inhomogeneous timber beams

¶
¶

Sigurdur Ormarsson
Department of Civil Engineering,
Technical University of Denmark, DK-2800 Lyngby, Denmark
Tel: +45 45 251738, Fax: +45 45 883282, E-mail:sor@byg.dtu.dk

Ola Dahlblom
Division of Structural Mechanics,
Lund University, Box 118, SE-221 00, Lund, Sweden

ABSTRACT

Wood is a hygro-mechanical, non-isotropic and inhomogeneous material concerning both modulus of elasticity (MOE) and shrinkage properties. In stress calculations associated with ordinary timber design, these matters are often not dealt with properly. The main reason for this is that stress distributions in inhomogeneous glued laminated members (glulams) and in composite beams exposed to combined mechanical action and variable climate conditions are extremely difficult to predict by hand. Several experimental studies of Norway spruce have shown that the longitudinal modulus of elasticity and the longitudinal shrinkage coefficient vary considerably from pith to bark. The question is how much these variations affect the stress distribution in wooden structures exposed to variable moisture climate. The paper presents a finite element implementation of a beam element with the aim of studying how wooden composites behave during both mechanical and environmental load action. The beam element is exposed to both axial and lateral deformation. The material model employed concerns the elastic, shrinkage, mechano-sorption and visco-elastic behaviour of the wood material. It is used here to simulate the behaviour of several simply-supported and continuous composite beams subjected to both mechanical and environmental loading to illustrate the advantages this can provide. The results indicate clearly both the inhomogeneity of the material and the variable moisture action occurring to have had a significant effect on the stress distribution within the cross-section of the products that were studied.

Key words: wood, moisture induced stresses, creep, FEM, beam element

1. INTRODUCTION

Solid timber is naturally suited as a source of members to be subjected to the combined effects of axial and flexural actions, since such solid members are sawn from the trunk of a tree. The high degree of stiffness and strength of the trunk in the axial direction makes the timber capable of withstanding high level of tension and of compression stress. Most structures and structural systems for building purposes consist of (solid or composite) beams, columns and frames that can be of differing types. The lamination and finger jointing of wood has also enabled timber beams and frames of virtually any length and shape to be produced. These products are usually graded higher than solid timber due to the fact that the natural and drying-related defects (such as knots, shakes and cracks) present in the wood material can be discarded.

During the last few decades extensive research has been carried out on material properties of wood and how these affect the quality and the surface performance of the final timber product. It is well

known, for example, that wood is very sensitive to climate changes in terms both of shrinking or swelling and of direct effects on its stiffness and strength properties [Bodig and Jayne (1982), Kollmann and Côté (1968), and Dinwoodie (1989)]. Wood is a hygroscopic material, meaning that it constantly attempts to come into equilibrium with climate conditions in the surroundings. This dynamic moisture process can result in solid timber and laminated timber products becoming markedly distorted (twisted, bowed, cupped or crooked) when they are exposed to climatic variation; see e.g. Johansson and Kliger (2002), Ekevad (2005), Ormarsson and Cown (2005), Astrup (2009) and Gereke et al. (2010). It is also well documented that wood is an inhomogeneous material concerning such parameters as the modulus of elasticity (MOE) [Dahlblom et al. (1999a)] and shrinkage coefficients in the fibre direction [Yamashita et al. (2009), and Dahlblom et al. (1999b)]. For normally grown trees, the MOE often increases quite linearly (up to factor of two) from pith to bark whereas the shrinkage coefficient usually decreases [Wormuth (1993), and Dahlblom et al. (1999b)]. It may be noted that variation in MOE and shrinkage properties is highly linked to the variation in the microfibril angle (MFA), high MFA results in low MOE and high shrinkage properties (see e.g. Persson 2000). For timber containing reaction wood, the inhomogeneity becomes stronger and the shrinkage or swelling is also considerably greater than for normal wood; see e.g. Ormarsson et al. (2000). The main reason for this is that the compression wood in general has much higher MFA than normal grown wood.

The fact that wood is an inhomogeneous material is not dealt with in EC5 more than in terms of encapsulation in connection with certain safety and modification factors. In textbooks on timber design; see e.g. Thelandersson and Larsen (2003), Porteous and Kermani (2007), and Larsen and Enjily (2009), it is often noted that the moisture sensitivity of the wood material needs to be taken into account and that structural timber should be dried (or conditioned) down to an average moisture content (MC) that corresponds to the expected climate conditions found during the service life of the wood product. In the EC5-rules for ultimate limit state (ULS) design, the moisture and load-duration effects on the strength properties of timber and wood-based products is dealt with by use of the modification factor k_{mod}. The values of the factor are based on three service classes representing different climate conditions and on five different duration-classes. For both solid timber and glued laminated timber, the k_{mod} values are similar for service classes 1 and 2 despite the differences between these two classes in terms of climate conditions. For the service limit state (SLS) design of EC5, the moisture effects on long-term deflection caused by creep is taken account of by means of the factor k_{def}, which predicts the larger deflections occurring in more humid environments. The problem here, however, is that natural moisture movements (shrinking and swelling) during the service life of the wood material can generate complex stress profiles (over the cross-section) that should better be taken into account in the process of designing timber structures. It is also interesting to study how mechano-sorption and creep deformations affect the stress distribution. Several experimental studies have been conducted to investigate how mechano-sorption and creep affect the deflection of wooden beams subjected to bending and to climate variation; see e.g. Bengtsson (2001), Bengtsson and Kliger (2003) and Mårtensson (1994).

Glued-laminated products consisting of inhomogeneous laminations to which MOE and shrinkage coefficients apply, as well as laminations of different strength classes, and laminations with differing moisture content when the final product is created, show a tendency for stresses to build up during changes in moisture level, due to the internal constraints that generate within the cross-section of the product. It is difficult, however, to predict how moisture-related stresses will develop during the service life of the product as a whole, especially if mechano-sorption effect and visco-elastic behaviour need to be taken account of as well. A simple finite element model was developed

with the aim of obtaining a better understanding of how (inhomogeneous) laminated products behave during combined mechanical and environmental loadings. It is a conventional beam model developed further so as to be able to simulate moisture related stresses in beams having an arbitrary number of inhomogeneous laminations. The wood lamellas are assumed to be fully fixed (glued) together, resulting in no-slip deformations along the glue lines. The MOE, the shrinkage coefficient and MC-changes can vary in an arbitrary manner within each lamella, which can result in discontinuous functions at the glue lines. The model is an incremental beam model that can predict the stress history as a whole of an arbitrary location within the beam. The material model employed deals with elastic, shrinkage or swelling, mechano-sorption and visco-elastic behaviour. The model (expanded beam theory) has been implemented in the finite element program CALFEM (2004).

2. THEORY

This section describes a finite element theory used for the simulation of inhomogeneous beams of wood. The longitudinal modulus of elasticity $E(x,y)$ and the longitudinal shrinkage coefficient $\alpha(x,y)$ are allowed to vary arbitrarily over the beam depth (y-coordinate) and along the element length (x-coordinate); see Fig. 1. All the material parameters are assumed to be constant across the beam z-direction. A beam element can be subjected to combined axial and uniaxial flexure (around the z-axis) as well as to environmental loading in terms of arbitrary variations in moisture content change $\Delta w(x,y)$ within the beam. The variation in moisture content changes over the cross section is e.g. affected by: different climate conditions at the beam surface, different MC states in the lamellae directly after gluing and different EMC and sorption isotherms for the lamellae. The material model employed deals with such phenomena as linear elasticity, shrinkage or swelling, mechano-sorption and visco-elastic wood behaviours.

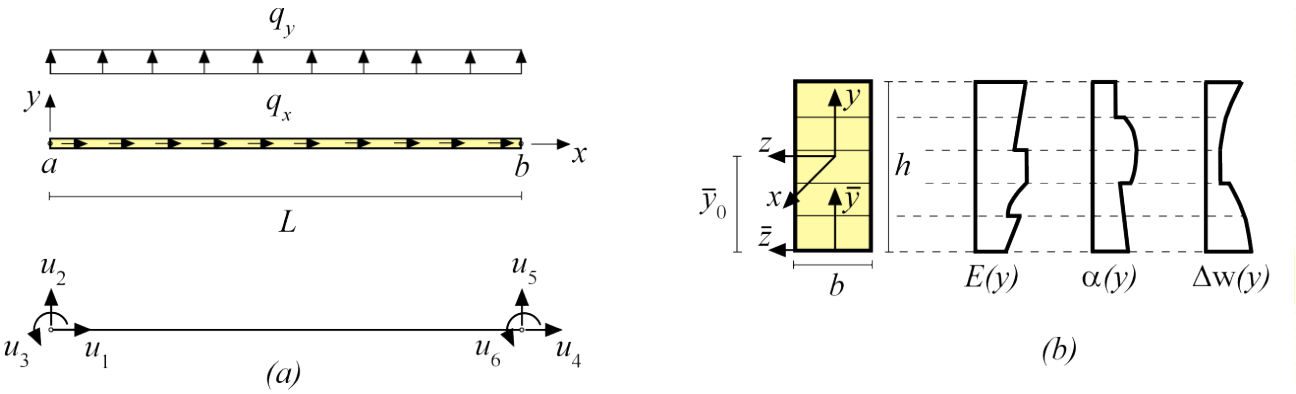

Figure 1. Diagram of the beam element studied:

(a) Geometry, loads and degrees of freedom

(b) Examples of how the modulus of elasticity $E(y)$, the shrinkage coefficient $\alpha(y)$ and the moisture content change $\Delta w(y)$ can vary across the depth of the cross-section.

2.1 The normal force centre (NFC) of the cross section

For markedly inhomogeneous cross sections (showing unsymmetrical variations in MOE across the depth of the beam) the normal force centre (NFC) and the centroid (C) can differ significantly in location within the cross-section. The NFC is the only point within the cross-section at which normal force action only generates extension or compression across the cross-section as a whole. In selecting the beam axis (origin of the cross-sectional coordinate system (y,z); see Fig. 1) at the NFC, the extension and the bending can be treated separately. For the coordinate system $(\bar{y}, \bar{z})$ the location of the NFC can be calculated as

$$\bar{y}_0(x) = \frac{D_{ES_{\bar{z}}}(x)}{D_{EA}(x)} \tag{1}$$

where

$$D_{ES_{\bar{z}}}(x) = \int_A E(x,\bar{y})\bar{y}dA \tag{2}$$

$$D_{EA}(x) = \int_A E(x,\bar{y})\, dA \tag{3}$$

The field $E(x,\bar{y})$ represents the effective modulus of elasticity in the beam direction. Based on the NFC location $\bar{y}_0(x)$, the field $E(x,\bar{y})$ can then be transformed to $E(x,y)$, which refers to the cross-sectional coordinate system. If the wood fibres are not oriented in the beam direction because of skewed sawing, spiral grain or some other misalignment, $E(x,y)$ can be calculated as

$$E(x,y) = \frac{1}{C_{11}(x,y)} \tag{4}$$

where C_{11} is the first diagonal value in the compliance matrix $\boldsymbol{C}$, referring to the global coordinate system (x,y,z). The transformation from the local coordinate system for the wood material directions (l,r,t) to the global one (x,y,z) is given by

$$\boldsymbol{C} = \boldsymbol{G}^{-1}\overline{\boldsymbol{C}}\boldsymbol{G}^{T^{-1}} \tag{5}$$

where $\boldsymbol{G}$ is the transformation matrix and $\overline{\boldsymbol{C}}$ is the compliance matrix referring to the local coordinate system (l,r,t) for wood being described in Ormarsson et al. (1998).

2.2 Constitutive relations

To simulate hygro-mechanical and (long-term) visco-elastic deformations in wood, the material model needs to take account of elastic, free shrinkage, mechano-sorption and visco elastic behaviour. For predicting the behaviour connected with mechano-sorption and creep, the theory needs to be expressed in an incremental form. The total strain rate in the beam direction is assumed to be the sum of four strain rates, i.e.

$$\dot{\varepsilon} = \dot{\varepsilon}_e + \dot{\varepsilon}_w + \dot{\varepsilon}_m + \dot{\varepsilon}_c \tag{6}$$

where a dot is a time derivative, ε is the total strain, ε_e the elastic strain, ε_w the moisture-induced strain, ε_m the mechano-sorption strain and ε_c the creep strain. The stress rate can be calculated as

$$\dot{\sigma} = E\dot{\varepsilon}_e = E(\dot{\varepsilon} - \dot{\varepsilon}_w - \dot{\varepsilon}_m - \dot{\varepsilon}_c) \tag{7}$$

The beam theory presented below needs to fulfil the beam specification termed *Bernoulli´s hypothesis* “The cross-sections are planar and perpendicular to the longitudinal material fibres before and after the deformation of the member”. This means that the total strain ε has to vary linearly over the cross sections whereas the strain portions $\varepsilon_e, \varepsilon_w, \varepsilon_m, \varepsilon_c$ can vary arbitrarily over the

cross sections. For an inhomogenous beam element (in the *xy*-plane) subjected to combined axial and bending action, the different strain distributions can be expressed as

$$\dot{\varepsilon}(x,y) = \dot{\varepsilon}_0(x) - \dot{\kappa}(x)y \tag{8}$$

$$\dot{\varepsilon}_w(x,y) = \widehat{\boldsymbol{G}}\dot{\boldsymbol{\varepsilon}}_w(x,y) = \widehat{\boldsymbol{G}}\boldsymbol{\alpha}(x,y)\dot{w}(x,y) \tag{9}$$

$$\dot{\varepsilon}_m(x,y) = \widehat{\boldsymbol{G}}\dot{\boldsymbol{\varepsilon}}_m(x,y) = \widehat{\boldsymbol{G}}\boldsymbol{m}\breve{\boldsymbol{G}}\sigma(x,y)\left|\dot{w}(x,y)\right| \tag{10}$$

$$\dot{\varepsilon}_c(x,y,t) = \widehat{\boldsymbol{G}}\dot{\boldsymbol{\varepsilon}}_c(x,y,t) = \widehat{\boldsymbol{G}}\sum_{n=1}^{N}\frac{1}{\tau_n}e^{-\frac{t}{\tau_n}}\dot{\bar{\boldsymbol{\gamma}}}_n(x,y,t) \tag{11}$$

where the rate of the creep driver $\dot{\bar{\boldsymbol{\gamma}}}_n(x,y,t)$ is given by the integral

$$\dot{\bar{\boldsymbol{\gamma}}}_n(x,y,t) = \int_0^t e^{\frac{t'}{\tau_n}}\overline{\boldsymbol{C}}_{c_n}\breve{\boldsymbol{G}}\dot{\sigma}(x,y,t')dt' =$$

$$\int_0^t e^{\frac{t'}{\tau_n}}\begin{bmatrix} \frac{1}{E_l(x,y)}\phi_n & -\frac{\nu_{rl}}{E_r}\phi_n & -\frac{\nu_{tl}}{E_t}\phi_n & 0 & 0 & 0 \\ -\frac{\nu_{lr}}{E_l}\phi_n & \frac{1}{E_r}\phi_n & -\frac{\nu_{tr}}{E_t}\phi_n & 0 & 0 & 0 \\ -\frac{\nu_{lt}}{E_l}\phi_n & -\frac{\nu_{rt}}{E_r}\phi_n & \frac{1}{E_t}\phi_n & 0 & 0 & 0 \\ 0 & 0 & 0 & \frac{1}{G_{lr}}\phi_n & 0 & 0 \\ 0 & 0 & 0 & 0 & \frac{1}{G_{lt}}\phi_n & 0 \\ 0 & 0 & 0 & 0 & 0 & \frac{1}{G_{rt}}\phi_n \end{bmatrix}\breve{\boldsymbol{G}}\dot{\sigma}(x,y,t')dt' \tag{12}$$

The matrices $\boldsymbol{\alpha}$ and $\boldsymbol{m}$ are shrinkage/swelling and mechanosorption matrices given in Ormarsson et al. (1998), matrix $\widehat{\boldsymbol{G}}$ being the first row in the inverse of the transformation matrix $\boldsymbol{G}^{-1}$ and $\breve{\boldsymbol{G}}$ being the transformation matrix $(\boldsymbol{G}^T)^{-1}$. The variables ϕ_n and τ_n are constants that describe the shape of the relative creep curve representing the whole service life of the studied products. The relative creep is calculated as a sum of different exponential functions becoming active during different time periods in the series; see Ormarsson et al. (2010) for more detailed description. The time t is the total time of the analysis, whereas t' represents different times at which the structure is subjected to new stress increments in terms of both mechanical and moisture action. For inhomogeneous (or unsymmetrical) cross sections in which the origin of the cross-sectional coordinate (y) is located at the NFC, the section force rate becomes

$$\begin{bmatrix} \dot{N}(x) \\ \dot{M}_z(x) \end{bmatrix} = \begin{bmatrix} D_{EA}(x) & 0 \\ 0 & D_{EI_z}(x) \end{bmatrix}\begin{bmatrix} \dot{\varepsilon}_0(x) \\ \dot{\kappa}_z(x) \end{bmatrix} - \begin{bmatrix} \dot{N}_p(x) \\ \dot{M}_{p_z}(x) \end{bmatrix} \tag{13a}$$

or

$$\dot{\boldsymbol{F}}(x) = \boldsymbol{D}(x)\dot{\boldsymbol{\zeta}}(x) - \dot{\boldsymbol{F}}_p(x) \tag{13b}$$

where $D_{EA}(x)$ and $D_{EI_z}(x)$ represent the axial and the bending stiffness of the cross section whereas $\dot{N}_p(x)$ and $\dot{M}_{p_z}(x)$ represent the incremental pseudo-section forces caused by free shrinkage strain, mechano-sorption strain and creep strain. These quantities are all cross-section related values given by

$$D_{EA}(x) = \int_A E(x,y)dA \tag{14}$$

$$D_{EI_z}(x) = \int_A E(x,y)y^2 dA \tag{15}$$

$$\begin{bmatrix} \dot{N}_p(x) \\ \dot{M}_{p_z}(x) \end{bmatrix} = \int_A E(x,y)\left(\begin{bmatrix} \dot{\varepsilon}_w(x,y) \\ \dot{\varepsilon}_w(x,y)y \end{bmatrix} + \begin{bmatrix} \dot{\varepsilon}_m(x,y) \\ \dot{\varepsilon}_m(x,y)y \end{bmatrix} + \begin{bmatrix} \dot{\varepsilon}_c(x,y) \\ \dot{\varepsilon}_c(x,y)y \end{bmatrix} \right) dA \tag{16a}$$

or

$$\dot{\boldsymbol{F}}_p(x) = \dot{\boldsymbol{F}}_w(x) + \dot{\boldsymbol{F}}_m(x) + \dot{\boldsymbol{F}}_c(x) \tag{16b}$$

For inhomogeneous beams, the variation in shear stress rate $\dot{\tau}(x,y)$ can be estimated by

$$\dot{\tau}(x,y) = \frac{\dot{V}\, D_{ES_z}^{A^*}(x,y)}{b(y)D_{EI_z}(x)} \tag{17}$$

where

$$D_{ES_z}^{A^*}(x,y) = \int_{A^*} E(x,y)ydA \tag{18}$$

and where V is a shear force caused by mechanical and moisture-related bending action, $D_{ES_z}^{A^*}(x,y)$ is the first moment of area (weighted by $E(x,y)$) above the shear stress level around the *z*-axis, $D_{EI_z}(x)$ is the bending stiffness as presented earlier, and *b(y)* is the width of the beam at the shear stress level.

2.3 Finite element formulation

As based on static equilibrium, the differential equations (strong form) for a beam subjected to axial and bending action is given by

$$\frac{dN}{dx} + q_x = 0 \qquad \text{(Axial action)} \tag{19}$$

$$\frac{d^2M_z}{dx^2} + q_y = 0 \quad \text{(Bending action around the major axis } z\text{)} \tag{20}$$

where the terms q_x, and q_y represent distributed loads acting in the x- and y-directions, respectively. The integral form (weak form) of these equations can be expressed as

$$\int_a^b \frac{dv_x}{dx} N dx - \left[v_x N\right]_a^b - \int_a^b v_x q_x dx = 0 \tag{21}$$

$$\int_a^b \frac{d^2 v_y}{dx^2} M_z dx - \left[\frac{dv_y}{dx} M_z\right]_a^b + \left[v_y V\right]_a^b + \int_a^b v_y q_y dx = 0 \tag{22}$$

Addition and differentiation of these expressions with respect to time yields the final (incremental) weak formulation in a matrix form as

$$\int_a^b (\tilde{\nabla}\boldsymbol{v})^T \dot{\boldsymbol{F}} dx - \left[(\hat{\nabla}\boldsymbol{v})^T \dot{\boldsymbol{F}}\right]_a^b + \left[\boldsymbol{v}^T \dot{\boldsymbol{V}}\right]_a^b - \int_a^b \boldsymbol{v}^T \dot{\boldsymbol{q}} dx = 0 \tag{23}$$

where

$$\tilde{\nabla} = \begin{bmatrix} \frac{d}{dx} & 0 \\ 0 & \frac{d^2}{dx^2} \end{bmatrix};\ \boldsymbol{v} = \begin{bmatrix} v_x \\ v_y \end{bmatrix};\ \hat{\nabla} = \begin{bmatrix} 1 & 0 \\ 0 & \frac{d}{dx} \end{bmatrix};\ \dot{\boldsymbol{F}} = \begin{bmatrix} \dot{N} \\ \dot{M}_z \end{bmatrix};\ \dot{\boldsymbol{V}} = \begin{bmatrix} 0 \\ \dot{V} \end{bmatrix};\ \dot{\boldsymbol{q}} = \begin{bmatrix} \dot{q}_x \\ -\dot{q}_y \end{bmatrix} \tag{24}$$

Based on the weak formulation given in Eq. (23) and the approximation $\boldsymbol{v} = \boldsymbol{N}\boldsymbol{c}$ for the arbitrary weight functions, the global FE-formulation can be expressed as

$$\int_a^b \boldsymbol{B}^T \dot{\boldsymbol{F}} dx - \left[(\hat{\nabla}\boldsymbol{N})^T \dot{\boldsymbol{F}}\right]_a^b + \left[\boldsymbol{N}^T \dot{\boldsymbol{V}}\right]_a^b - \int_a^b \boldsymbol{N}^T \dot{\boldsymbol{q}} dx = 0 \tag{25}$$

where $\boldsymbol{N}$ is the shape function matrix, $\boldsymbol{c}$ is an arbitrary constant vector and $\boldsymbol{B} = \tilde{\nabla}\boldsymbol{N}$. Insertion of the constitutive relation (13b) yields

$$\int_a^b \boldsymbol{B}^T (\boldsymbol{D}\dot{\boldsymbol{\zeta}} - \dot{\boldsymbol{F}}_p) dx - \left[(\hat{\nabla}\boldsymbol{N})^T \dot{\boldsymbol{F}}\right]_a^b + \left[\boldsymbol{N}^T \dot{\boldsymbol{V}}\right]_a^b - \int_a^b \boldsymbol{N}^T \dot{\boldsymbol{q}} dx = 0 \tag{26}$$

The total strain/curvature vector $\dot{\boldsymbol{\zeta}}$ can be expressed as

$$\dot{\boldsymbol{\zeta}} = \tilde{\nabla}\dot{\boldsymbol{u}} = \tilde{\nabla}\boldsymbol{N}\dot{\boldsymbol{a}} = \boldsymbol{B}\dot{\boldsymbol{a}} \tag{27}$$

where $\boldsymbol{u} = [u\ v]^T$ is the displacement vector and $\boldsymbol{a}$ is the global nodal displacement/rotation vector. Insertion of Eq. (27) into Eq.(26) yields

$$\int_a^b \boldsymbol{B}^T \boldsymbol{D}\boldsymbol{B} dx \dot{\boldsymbol{a}} - \left[(\hat{\nabla}\boldsymbol{N})^T \dot{\boldsymbol{F}}\right]_a^b + \left[\boldsymbol{N}^T \dot{\boldsymbol{V}}\right]_a^b - \int_a^b \boldsymbol{N}^T \dot{\boldsymbol{q}} dx - \int_a^b \boldsymbol{B}^T \dot{\boldsymbol{F}}_p dx = 0 \tag{28}$$

Based on the above expression, the finite element equation becomes

$$\boldsymbol{K}\dot{\boldsymbol{a}} = \dot{\boldsymbol{f}}_b + \dot{\boldsymbol{f}}_l + \dot{\boldsymbol{f}}_p \tag{29}$$

where

$$\boldsymbol{K} = \int_a^b \boldsymbol{B}^T \boldsymbol{D}\boldsymbol{B} dx \qquad \text{(Stiffness matrix)} \tag{30}$$

$$\dot{\boldsymbol{f}}_b = \left[(\hat{\nabla}\boldsymbol{N})^T \dot{\boldsymbol{F}}\right]_a^b - \left[\boldsymbol{N}^T \dot{\boldsymbol{V}}\right]_a^b \qquad \text{(Boundary vector)} \tag{31}$$

$$\dot{\boldsymbol{f}}_l = \int_a^b \boldsymbol{N}^T \dot{\boldsymbol{q}} dx \qquad \text{(Load vector)} \tag{32}$$

$$\dot{\boldsymbol{f}}_p = \dot{\boldsymbol{f}}_w + \dot{\boldsymbol{f}}_m + \dot{\boldsymbol{f}}_c = \int_a^b \boldsymbol{B}^T \dot{\boldsymbol{F}}_p dx = \int_a^b \boldsymbol{B}^T (\dot{\boldsymbol{F}}_w + \dot{\boldsymbol{F}}_m + \dot{\boldsymbol{F}}_c) dx \qquad \text{(Pseudo-load vector)} \tag{33}$$

where $\dot{\boldsymbol{f}}_w$, $\dot{\boldsymbol{f}}_m$ and $\dot{\boldsymbol{f}}_c$ are the pseudo-load vectors for free shrinkage, mechano-sorption and creep strain, respectively. For a planar beam element (with 6 degrees of freedom, see Fig 1*(a)*), the element displacement/rotation vector $\boldsymbol{a}^e$, the element shape function matrix $\boldsymbol{N}^e$ and the associated strain/curvature matrix $\boldsymbol{B}^e$ are given by

$$\boldsymbol{a}^e = \begin{bmatrix} u_1 & u_2 & u_3 & u_4 & u_5 & u_6 \end{bmatrix}^T \tag{34}$$

$$\boldsymbol{N}^e = \begin{bmatrix} N_1^e & 0 & 0 & N_4^e & 0 & 0 \\ 0 & N_2^e & N_3^e & 0 & N_5^e & N_6^e \end{bmatrix} \tag{35}$$

$$\mathbf{B}^e = \tilde{\nabla}\boldsymbol{N}^e = \begin{bmatrix} \dfrac{dN_1^e}{dx} & 0 & 0 & \dfrac{dN_4^e}{dx} & 0 & 0 \\ 0 & \dfrac{d^2N_2^e}{dx^2} & \dfrac{d^2N_3^e}{dx^2} & 0 & \dfrac{d^2N_5^e}{dx^2} & \dfrac{d^2N_6^e}{dx^2} \end{bmatrix} \tag{36}$$

where the shape functions for the axial and flexural deformation are

$$N_1^e = -\frac{1}{L}(x-L);\ \ N_4^e = \frac{1}{L}x \tag{37}$$

$$N_2^e = 1 - 3\frac{x^2}{L^2} + 2\frac{x^3}{L^3};\ \ N_3^e = x\left(1 - 2\frac{x}{L} + \frac{x^2}{L^2}\right);\ \ N_5^e = \frac{x^2}{L^2}\left(3 - 2\frac{x}{L}\right);\ \ N_6^e = \frac{x^2}{L}\left(\frac{x}{L} - 1\right) \tag{38}$$

3. NUMERICAL EXAMPLES

The beam theory presented above has been implemented in the finite element software CALFEM, which is an FE-toolbox in the Matlab environment; see CALFEM (2004). The beam model is a finite element model suitable for simulation of hygro- and visco-elastic behaviours in inhomogeneous structural timber elements (beams, columns and frames). It is an incremental model

that can deliver historical output for displacements and rotations (v, ϕ), section forces (M, V, N), curvatures and strains (κ, ε) and stresses (σ, τ) during the service life of the structure. All integral expressions concerning variation over the cross section of the beam or along it are performed using numerical integration. The material parameters in addition to $E(y)$ and $\alpha(y)$ are the same as used in Ormarsson (1999). The creep data employed is based on experimental work presented by Gressel (1984). Additional information concerning the relative creep curve can be found in Ormarsson et al. (2010).

3.1 Simply supported beam

A laminated I-beam consisting of three solid wood lamellae was used to study how variations in the modulus of elasticity $E(y)$ and the shrinkage coefficient $\alpha(y)$ affect the cross-sectional stress pattern in laminated timber products. The beam was 3 m long and simply supported. It functioned as a typical composite beam since the laminations were assumed to be assembled by gluing, so that no slip deformation between the lamellae would arise. The cross-sectional dimensions and the curves representing variation in $E(y)$, $\alpha(y)$ and $\Delta w(y)$ are shown in Fig. 2. For the flange members, $E(y)$ and $\alpha(y)$ vary linearly over the cross-section, whereas they are evenly distributed within the web. Each of the members is exposed to a constant moisture change $\Delta w = -4\%$ (drying). Figure 2 shows two stress profiles, the first one (Sim.1) presenting a linear elastic stress response occurring directly after drying, the second one (Sim. 2) showing a stress profile as it appeared after 50 years. The entire drying process (4%) was assumed to occur during the first year of service life, whereas the creep deformation, in contrast, developed over a period of 50 years. The mechano-sorption effect had only a slight effect on stress profile 2, since the normal stresses were rather slight and the drying was also limited. Generally, the mechano-sorption effect in wood is relatively small in the fibre direction (l) as compared to what happens in the other material directions (r, t). The results show the maximum tensile stress (approx. 1.7 MPa) present at the boundary between the flanges and the web. At these locations the stress jumps from about 1.7 MPa in tension to about -0.7 MPa in compression. The stress jumps occur because the $E(y)$ and $\alpha(y)$ curves being discontinuous at these locations.

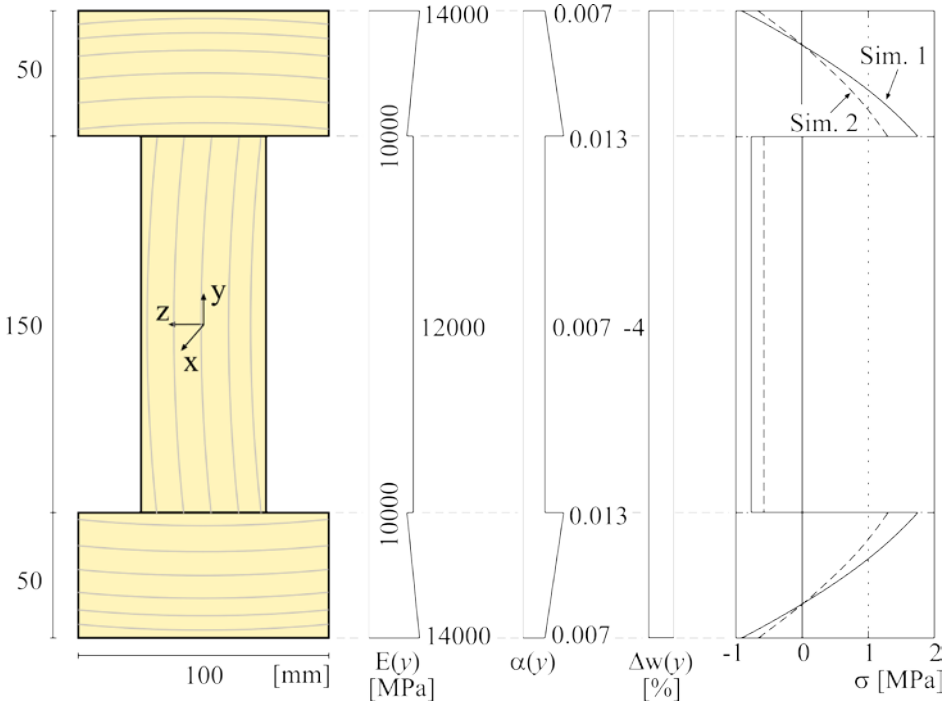

Figure 2. Stress distribution in an inhomogeneous simply-supported I-beam exposed to constant change in moisture content ($\Delta w = -4\%$).

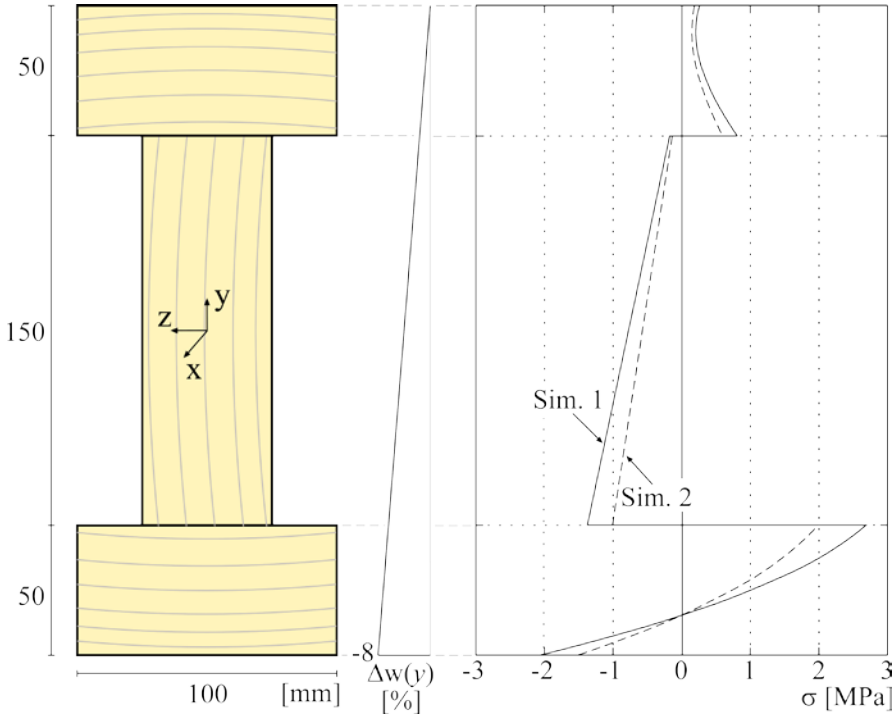

Figure 3. Stress distribution in an inhomogeneous simply-supported I-beam exposed to a linearly distributed change in moisture content over the cross section, ($E(y)$ and $\alpha(y)$ are the same functions as in Fig. 2).

The stress curves within the flanges are quadratic because of the linear variations in $E(y)$ and $\alpha(y)$ that occurred. The stress profile is symmetrical since the input data shows symmetrical variation over the cross-section. The stress distribution also implies that the normal force, the moment and the curvature become zero. When the material shrinks or swells, an internal constraint is generated due to the inhomogeneity of the shrinkage parameters. There is also a stress reduction due to the creep deformation that takes place despite there being no axial displacement or flexure. The creep model used is a linear Kelvin model in terms of which the creep effect is proportional to the stress state in the material. Figure 3 shows stress profiles for the same I-beam as presented in Fig. 2. It is exposed to linearly distributed changes in moisture content over the cross section, i.e. 8% drying at the bottom edge down to zero at the top edge. For both simulations, the beam became bent having a constant curvature of $\kappa = -0.0029$ m^{-1} and a maximum deflection of v_{max}= 3.3 mm. Since the beam was simply-supported (statically determinate) and was only exposed to environmental loading, the moment and the normal force became zero. The maximum tensile stress is about 2.7 MPa at the boundary between the bottom flange and the web. The stress curves within the flanges are curved whereas they are linear functions within the web. The maximum jumps in the stress curves occur at the same location as the maximum tensile stresses. As before, the stress is reduced due to the creep deformation that occurs, despite the total deformation being unchanged.

Figure 4 shows stress results for the I-beam when it is exposed to a linearly distributed change in moisture content across the flanges, resulting in drying in the bottom flange and moistening in the top flange. The beam becomes bent, having a constant curvature of $\kappa = -0.0025$ m^{-1} and a maximum deflection of v_{max}= 2.8 mm. The maximum stress becomes almost 3.0 MPa in compression at the boundary between the bottom flange and the web. As in the previous example, the stress graphs are curved within the flanges and linear in the web, the maximum stress jumps occurring at the same location as the maximum stresses, the creep deformation reducing the stresses despite the total deformation of the beam being unchanged, the moment and the normal force also being zero.

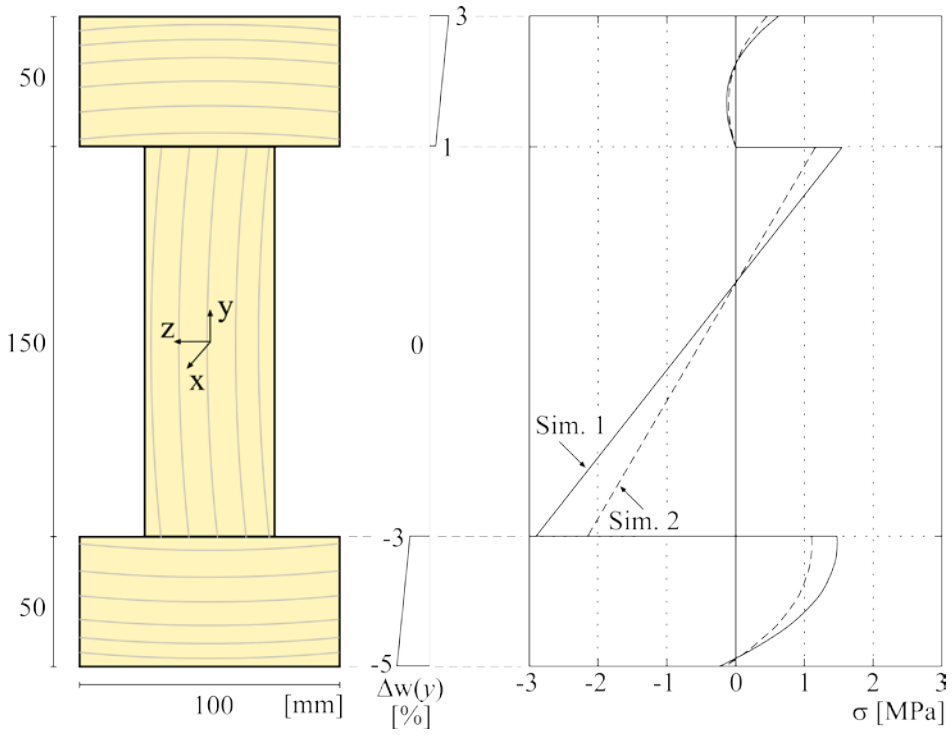

Figure 4. Stress distribution in an inhomogeneous simply-supported I-beam exposed to a linearly distributed change in moisture content within the flanges and to no moisture change within the web, ($E(y)$ and $\alpha(y)$ being the same functions as in Fig. 2).

3.2 Continuous beam

To study how structural constraints affect the stress distribution, a continuous I-beam spanning two 3 m long spans was studied. Both the material data and the changes in moisture content were the same as for the beam shown in Fig. 4. Stress variations (with and without creep) over the cross-section above the middle support are shown in Fig. 5. The maximum stresses there were now

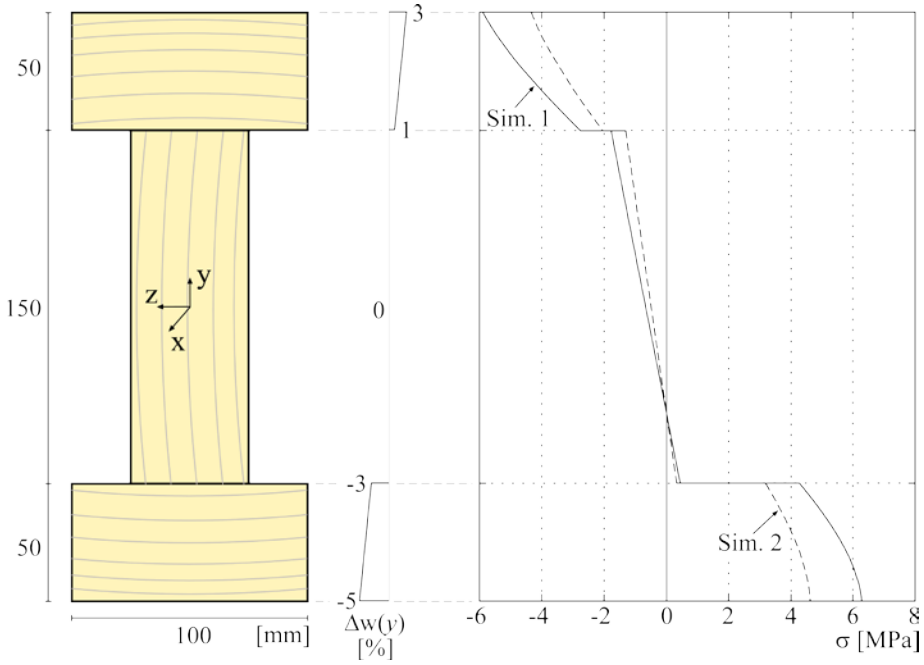

Figure 5. Stress distribution in an inhomogeneous two-span I-beam exposed to the same changes in moisture content as shown in Fig. 4, ($E(y)$ and $\alpha(z)$ being the same functions as in Fig. 2).

approximately 6.0 MPa in both tension and compression, the maximum stresses being located at the top and at the bottom surfaces of the flanges. As before the stress graphs are curved within the flanges and linear within the web. Note that in this case the maximum stresses are up to 40% of the design strength of solid timber of strength class C24 subjected to a medium load-duration, despite the change in moisture content being relatively small. Since the beam is statically indeterminate,

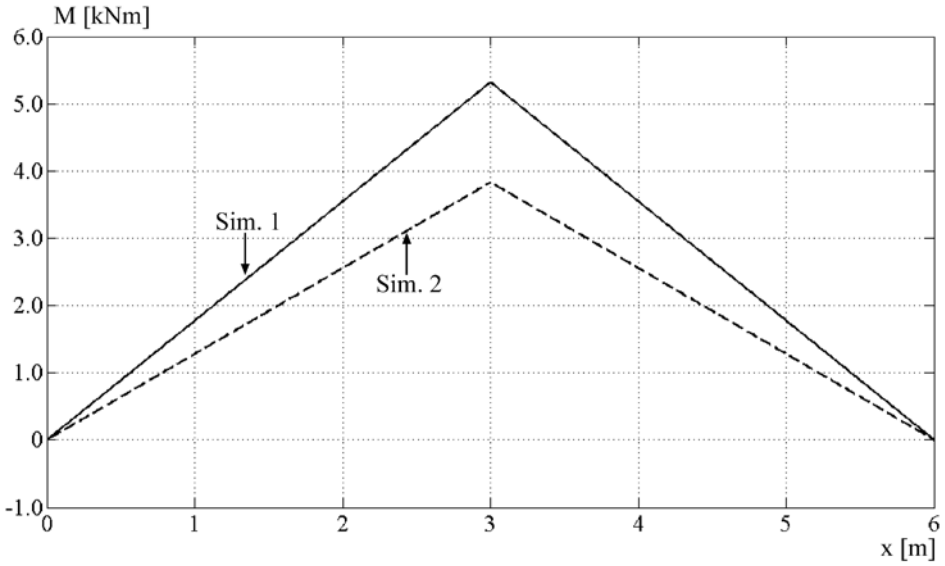

Figure 6. Moment distribution along the I-beam presented in Fig. 5, ($E(y)$ and $\alpha(y)$ are the same functions as in Fig. 2).

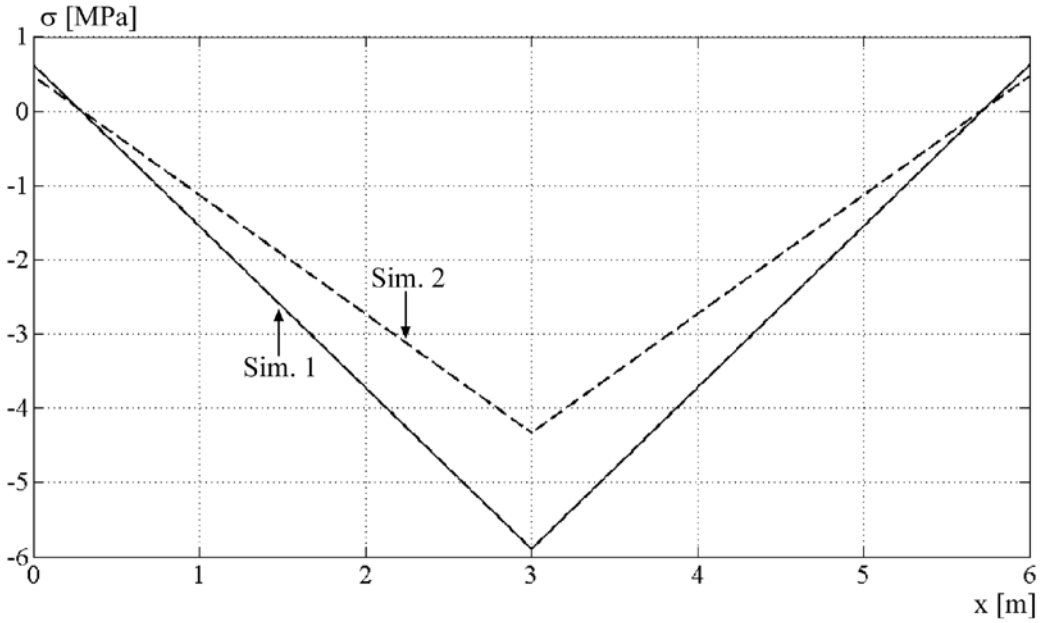

Figure 7. Stress distribution along the top surface of the I-beam shown in Fig. 5, (E(z) and $\alpha(z)$ being the same functions as in Fig. 2).

moment variation is built up along the beam. Figures 6 and 7 show how the moment and the stresses at the top surface vary linearly along the beam. The moment is zero at the end supports and increases linearly to about 5.3 kNm above the middle support. Again, this is a major moment, one that is generated by a relatively small change in moisture content in combination with one structural constraint (the middle support). The moment becomes so large because of the beam striving to bend upwards while it is fixed in position at the middle support. The stresses at the top surface vary in a

manner similar to the moment to maximum compression stress of about -6 MPa present at the middle support. Both the moment and the stresses were reduced significantly because of creep deformation. Figure 8 shows the deflection curve of the beam, which displays about the same deflection before as after creep deformation. Thus, the reduction in the elastic strain is of about the same magnitude as the increase of the creep strain. The maximum deflection is slightly above 0.8 mm (upwards) in the middle of the spans and zero at the supports.

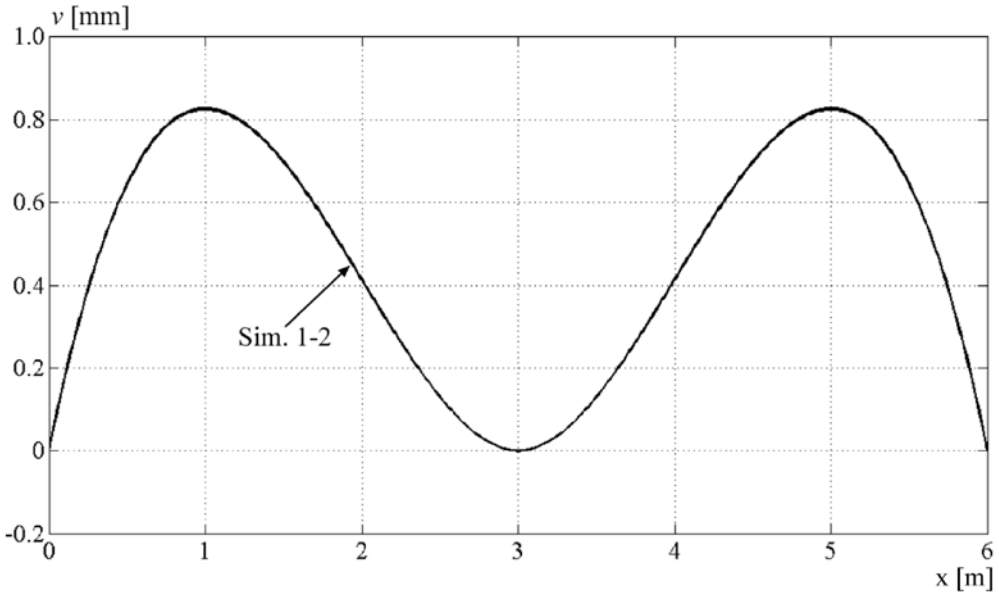

Figure 8. Deflection of the continuous I-beam presented in Fig. 5, ($E(y)$ and $\alpha(y)$ are the same functions as in Fig. 2).

3.3 Glulam beam

The final example given presents simulation results for a glulam beam subjected to combined mechanical flexure and environmental loading. The beam is a 3 m long and simply-supported beam having a cross-section of six 45x100 mm lamellae. It is loaded with an evenly distributed line load $q_d = -8.0$ kN/m along the beam. Figure 9 shows four different stress profiles over the cross-section of the beam. The first two simulations (Sim. 1 and Sim. 2) show an elastic stress distribution caused by the distributed load for a beam with a constant E = 14,000 MPa and one for a beam with a linear variation in the E-modulus within each lamella, extending from 12,000 MPa on the bottom side to 16,000 MPa on the top side. Typical linear variation was found for the first simulation and a slightly curved and discontinuous curve for the second simulation. The jumps occurred at the boundaries between the lamellae, where the discontinuity in the modulus of elasticity was found. On the top side, the stresses increased from about 7.0 MPa in the first simulation to about 9.0 MPa in the second one. This increase took place because of the modulus of elasticity having its maximum value on the top surface of the lamellae. Note that the deflection presented in Figure 11 shows about the same flexure in both of these simulations. In the third simulation (Sim. 3), the top lamella was exposed to 2% moistening and the lamella below to 2% drying. This could have occurred through the lamellae that were glued together differing in their moisture content. This moisture loading increased the stress on the top surface from 9.0 MPa to about 11.5 MPa. Thus, the maximum stress in the first simulation (for a constant E-modulus) increased by 55%. This indicates clearly how important it is to take the inhomogeneity (variation in the E-modulus) of the wood material and the moisture related loading into account. The last simulation (Sim. 4) shows the stress profile after 50 years of creep deformation. The stress reduction is greatest in the two top lamellae, where the moisture-related stresses are largest. Note that the creep deformation has no effect on stresses caused by mechanical load.

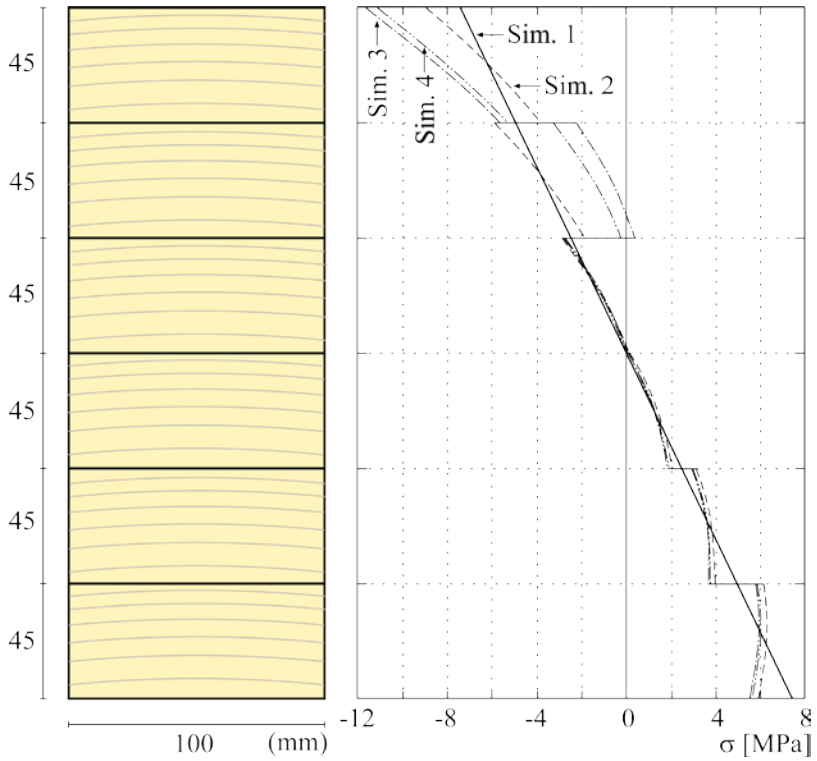

Figure 9. Stress distribution in a glulam beam:
Sim 1: constant *E*-modulus E = 14000 MPa and distributed load $q_d = -8.0$ kN/m;
Sim 2: $E(y)$ varying linearly from 12000 to 16000 MPa, the mechanical load being the same as in Sim.1;
Sim 3: Sim. 2 exposed to an additional 2% of moistening of the top lamella and a 2% drying of the lamella below;
Sim 4: Sim. 3 plus the creep deformation that occurred during a period of 50 years.

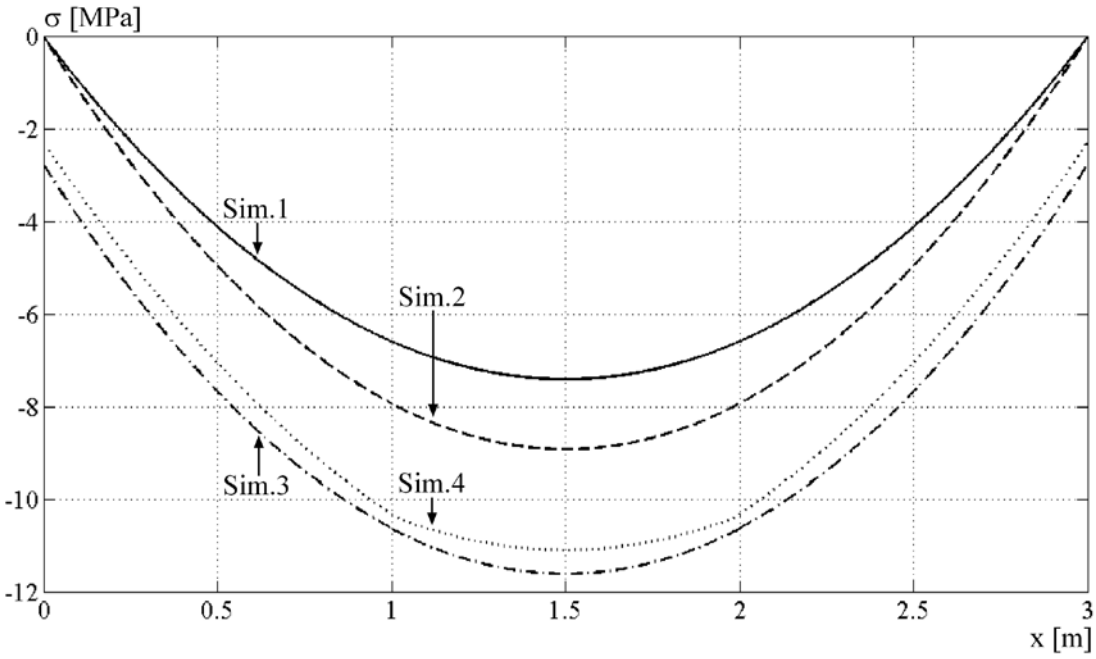

Figure 10. Variations in stress along the top surface of the glulam beam shown in Fig. 9.

Figure 10 shows the variation in stress along the top edge of the beam. It illustrates clearly how the stress increases from the first simulation to the third, and the constant reduction in stress due to creep deformation (Sim. 4). It also shows that the stresses in simulations 3 and 4 are not zero at the ends of the beam. The reason for this is that the beam theory only requires the normal force and the moments but not the stresses to be zero at the supports.

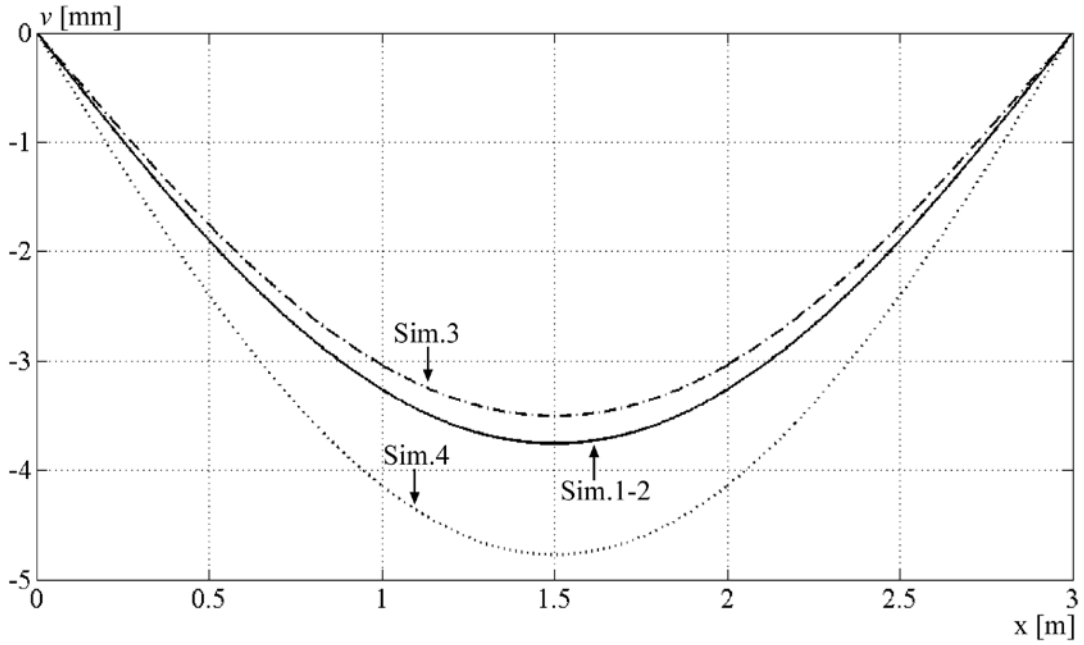

Figure 11. Deflection graphs of the glulam beam shown in Fig. 9.

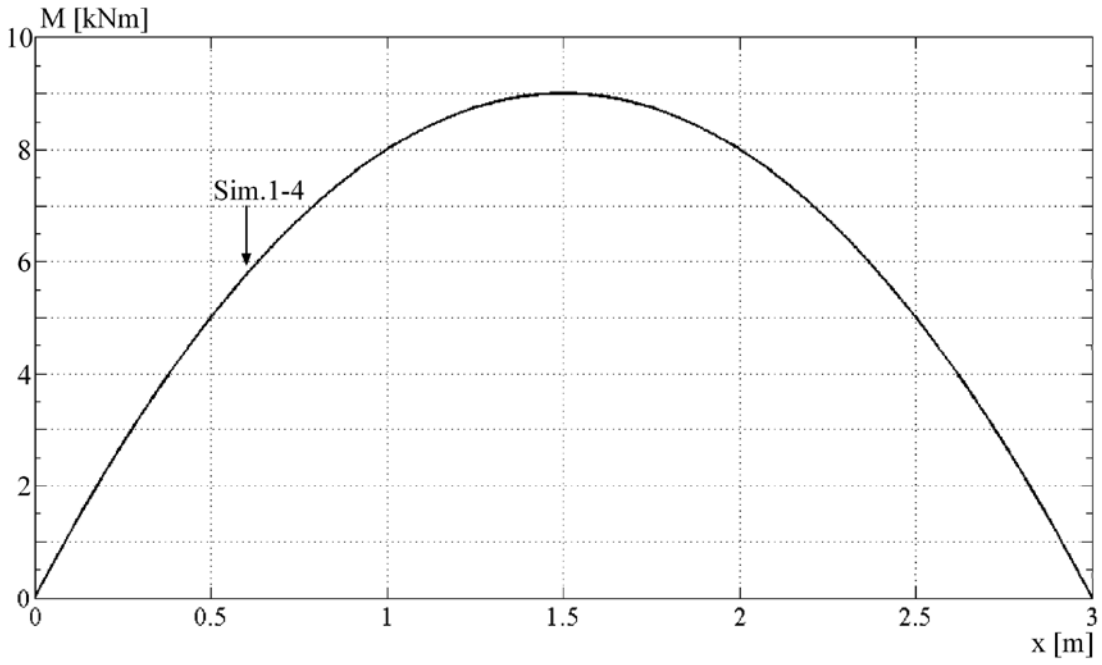

Figure 12. Moment variation along the glulam beam shown in Fig. 9.

The deflection of the beam is shown in Fig. 11. The first and the second simulation (Sim. 1-2) shows about the same deflection. This is because the constant modulus of elasticity in the first simulation was the average value of the modulus of elasticity variation in the second one. The

deflection is reduced slightly when the beam is subjected to the moisture load since the moisturising of the top lamella tends to produce upward deflection. The creep deformation in simulation four causes considerable deflection because of the strong bending action caused by the distributed load.

Figure 12 shows the moment distribution along the beam. It displays clearly the same moment distribution as in all the simulations. Since the beam is statically determined, the moment is caused only by the mechanical load, which results in a maximum moment of M_{max} = 9.0 kNm at the centre of the beam and a zero moment at the supports.

4. DISCUSSION AND CONCLUSIONS

¶

For composite beams, the approach of employing the modular ratio is commonly used in timber design because of the differences in stiffness of the laminations. However, if the composites are exposed to variable changes in moisture, the theory involved becomes very complex, especially if the composites are assumed to be inhomogeneous regarding their stiffness and shrinkage properties. The numerical results presented in the paper show that the finite element theory for the beam element studied can be used successfully for simulating combined elastic, hygro-mechanical and visco-elastic behaviour in inhomogeneous laminated timber beams. Adequate knowledge of the stiffness, shrinkage or swelling, and creep properties involved is needed, however, to obtain satisfactory simulation results for variations in stress over the cross-section. The model is small (in terms of number of degrees of freedom), flexible and effective and can easily be developed further for more complex behaviours and cross-sectional geometries. If one has information available concerning variations in climate over a long period in time, the model can be used to study how timber structures behave (in terms of deflection, creep and stresses) during their service life as a whole. The particular advantage of the model is thus that it can simulate complex behaviour with use of very limited computer power.

The results of the simulation show that moisture-related stresses can become relatively large even when there is only a limited change in moisture content within the wood lamellae. Since the variations in stress over the cross-section can also be quite complex (their being both nonlinear and discontinuous), it is difficult to know where the maximum stress will be located. Variations in the modulus of elasticity also have a significant effect on the stress profile, the maximum stress value increasing. The computations made also provided interesting results regarding the interaction between creep, moisture-related stress, boundary conditions and structural constraints.

On the basis of the numerical results presented, it can be concluded that knowledge of material inhomogeneity and of stresses caused by changes in climate should be taken more careful account of in the process of designing timber structures. There is a strong need for simple and effective simulation tools being developed, in particular for advanced timber design. The importance of this type of modelling is that it makes it possible to analyse statically indeterminate trusses and frame structures exposed to combined mechanical and environmental loading during their whole service life. The theory has also a high potential to be developed further for curved timber structures and composite beams with nailed longitudinal joints. The theory is needed within the field of timber engineering to better understand the climate related and long term structural behaviour of timber structures. It can be implemented for practical use through user-friendly software which can be a step forward in the process to implement this type of load actions in the future timber standards.

¶

5. FUTURE WORK

¶

The beam model presented can be developed further, for example regarding more complex cross-sectional geometries, variations in geometry along the beam $A(x)$, biaxial bending, arbitrary

variation in $E(x,y,z)$ and $\alpha(x,y,z)$ over the cross-section, curved annual rings, twist deformation and geometrical nonlinearity. Until now, the moisture content history for the cross-section involved has been given as known input data. To obtain better predictions of the moisture history, it could instead be simulated by a two-dimensional moisture flow analysis coupled with the beam stress analysis. It would also be possible to develop the beam element further for simulation of beams having mechanical joints that allow small slip deformations to occur. In addition, the material model could also be expanded so as to include a non-linear visco-elastic model and finite shear deformations.

References

[1] Astrup T. *Numerical modeling of deformations in wood*, Doctoral Thesis, Report R-217, Technical University of Denmark, Dep. of Civil Engineering. Kgs. Lyngby, Denmark; 2009.

[2] Bodig J, Jayne B. A. Mechanics of wood and wood composites, Van Nostrand Reinhold Company, New York; 1982.

[3] Bengtsson C. Short-term mechano-sorptive creep of well-defined spruce timber. *Holz als Roh- und Werkstoff*, 2001;59:117-128.

[4] Bengtsson C., Kliger R. Bending creep of high-temperature dried spruce timber, *Holzforschung*, 2003;57:95–100.

[5] CALFEM, A finite element toolbox to MATLAB, Version 3.4; 2004 http://www.byggmek.lth.se/Calfem.

[6] Dahlblom O., Petersson H., Ormarsson S. Characterization of modulus of elasticity, European project FAIR CT 96-1915, Improved Spruce Timber Utilization, Final report Sub-task AB1.7; 1999a.

[7] Dahlblom O., Petersson H., Ormarsson S. Characterization of shrinkage, European project FAIR CT 96-1915, Improved Spruce Timber Utilization, Final report Sub-task AB1.5; 1999b.

[8] Dinwoodie J.M. Timber, its nature and behaviour, Van Nostrand Reinhold Company, New York; 1981.

[9] Ekevad M. Twist of wood studs: dependence on spiral grain gradient, *J Wood Sci*, 2005;51:455–461.

[10] Gereke T., Hass P. and Niemz P. Moisture-induced stresses and distortions in spruce cross-laminates and composite laminates, *Holzforschung*, 2010;64(1):127–133.

[11] Gressel P. Zur Vorhersage des langfristigen Formänderungsverhaltens aus Kurz-Kriechversuchen. *Holz Roh Werkst*, 1984;42:293–301.

[12] Johansson, M. Kliger, R. Influence of material characteristics on warp in Norway spruce timber. *Wood and Fibre Science*, 2002;34(2): 325-336.

[13] Kollmann F. F. P., Côté Jr. W. A. Principles of Wood Science and Technology. I. Solid Wood, Springer-Verlag, Berlin; 1968.

[14] Larsen H. J. and Enjily V. Practical design of timber structures to Eurocode 5, Thomas Telford Ltd, UK; 2009.

[15] Mårtensson A. Creep behavior of structural timber under varying humidity conditions**,** *Journal of Structural Engineering*, 1994;Vol. 120, No. 9.

[16] Ormarsson S. *Numerical Analysis of Moisture-Related Distortion in Sawn Timber*, Doctoral Thesis, Publ 99:7, Chalmers University of Technology, Dep. of Structural Mech. Göteborg, Sweden; 1999.

[17] Ormarsson S., Dahlblom O. and Petersson H. A numerical study of the shape stability of sawn timber subjected to moisture variation. Part 1: Theory. *Wood Science and Technology*, 1998; 32:325-334.

[18] Ormarsson S. and Cown D. Moisture-Related Distortion of Timber Boards of Radiata Pine: Comparison with Norway Spruce, *Wood and Fiber Science*, 2005;37(3):424-436.

[19] Ormarsson S., Dahlblom O. and Johansson M. Numerical study of how creep and progressive stiffening affect the growth stress formation in trees, *Trees – Structure and Function*, 2010;Vol 24, issue 1:105-115.

[20] Ormarsson S., Petersson H. and Dahlblom D. A numerical and experimental study of compression wood influence on drying timber distortion. Drying Techn. - *An Int. Journal. - Special Issue on Wood Drying*, 2000;18:8:1897-1919.
[21] Persson K. *Micromechanical modelling of wood and fibre properties*, Doctoral thesis, Publ. TVSM-1013, Div. of Struc. Mech., Lund University, Sweden; 2000.
[22] Porteous J., Kermani A. Structural Timber Design to Eurocode 5, Blackwell Publishing Ltd, UK; 2007.
[23] Thelandersson S. and Larsen H. J. Timber Engineering, John Wiley & Sons Ltd, England; 2003.
[24] Yamashita K., Hirakawa Y., Nakatani H. and Motoyoshi I. Longitudinal shrinkage variations within trees of sugi (Cryptomeria japonica) cultivars. *J Wood Sci*, 2009;55:1–7.
[25] Wormuth E-W. Study of the relation between flatwise and edgewise modulus of elasticity of sawn timber for the purpose of improving mechanical stress methods. Diploma work, University of Hamburg, Department of Wood Technology, Hamburg; 1993.